RSC Advances

ROYAL SOCIETY OF CHEMISTRY

www.rsc.org/advances

Journal Name

RSCPublishing

ARTICLE

A Novel Approach to Prepare Polymer Mixed-Brushes via Single Crystal Surface Patterning*

Cite this: DOI: 10.1039/xoxxoooooo

S. Abbaspoor, F. Abbasi and S. Agbolaghi

Received ooth January 2014,
Accepted ooth January 2014

DOI: 10.1039/xoxxoooooo

www.rsc.org/

Polymer mixed-brushes with predetermined morphologies as well as uniform chain length and chain length distribution of various brushes were prepared on a substrate via single crystal surface patterning with the self-seeding procedure from a dilute solution. The required materials comprising poly(ethylene glycol)-*b*-polystyrene (PEG-*b*-PS) and poly(ethylene glycol)-*b*-poly(methyl methacrylate) (PEG-*b*-PMMA) with the same molecular weight of crystalline block and different molecular weights of amorphous blocks were synthesized via atom transfer radical polymerization (ATRP). Based on various qualities of employed solvent and different interactions of substrate with amorphous blocks, the matrix (PS)-dispersed (PMMA) morphologies could be obtained on the PEG single crystals. The matrix and dispersed phase regions were detectable by atomic force microscopy (AFM) due to having different heights and stiffnesses. The domain size of dispersed phase decreased with enhancing the molecular weights of PS and PMMA blocks, for hindrance increase against presence of PEG-*b*-PMMA chains. Despite ranging the domain size of the dispersed phase from 286 to 351 nm, the crystallization temperature was not effective on it significantly. Through rising the crystallization temperature, the thickness and, consequently, the tethering density enhancement was more considerable for PS regions, and it could be attributed to the lower osmotic pressure of PS chains. Finally, we grew the epitaxial structures consisting PEG-*b*-PS, PEG-*b*-PMMA, and homo-PEG layers to verify the determined thicknesses from mixed-brush systems through the conjunction thickness of corresponding copolymer and homopolymer crystals.

Introduction

In order to apply the materials in various applications of industry, nanotechnology, and biomedicine, the surface properties of materials should be modified [1-5]. Up to now, different methods which fall into categories of mechanical techniques, monolayer adsorption, plasma treatment, chemical coatings and use of polymer chains have been applied to modify the surfaces [3,4,6,7]. Duo to high sensitivity of polymers to the lowest environmental variations, polymer brushes are considered as the best candidate for surface modification applications [4,8-16]. This property provides an opportunity to bring them in use of many applications. For some instances, biomaterials, microfluidic devices, tissue engineering, membrane surface modification, colloidal stabilization, chemical sensors, and ion-exchange adsorbents [9,17-28]. To obtain a combination of various properties for a surface-grafted monolayer, the polymer mixed-brushes could be fabricated. Due to presence of different polymer brushes having various behaviours in mixed-brush structures, they are capable to introduce wide range of morphologies as well as responses [9,20,29,30]. To construct the polymer mixed-brush surface morphologies, various methods such as grafting to, grafting from, combination of both and single crystal growth of star block copolymers have previously been presented [9,20,30-37]. The single crystal growth method, which is able to produce the homogeneous brush length and length distribution and to adjust accurate grafting density, has priority to others [37-40].

In our novel approach, the mixed-brush single crystals were grown from dilute solution including two amorphous-crystalline diblock copolymer chains with the same crystalline block. Our surface patterning is a random pattern, a kind of leopard skin. We had access to true control of poly(methyl methacrylate) (PMMA)-dispersed domain (playing the role of spread patches) size in the PS-matrix but the population of them was not exactly predictable on a given surface area of single crystal. In this work, we have employed the materials [poly(ethylene glycol)-*b*-polystyrene (PEG-*b*-PS)/poly(ethylene glycol)-*b*-poly(methyl methacrylate) (PEG-*b*-

Institute of Polymeric Materials, Sahand University of Technology, Tabriz, Iran. E-mail: f.abbasi@sut.ac.ir

*Electronic Supplementary Information (ESI) available: [details of any supplementary information available should be included here]. See DOI: 10.1039/b000000x/

PMMA)] with the weight ratio of 50/50. Furthermore, the lateral habit of grown single crystals was investigated elsewhere [41].

Here, the main reason to select the PS and PMMA amorphous blocks was their different compatibilities with PEG crystalline block. Upon constructing the PEG substrate, although the interaction of PMMA brushes with it is attractive, the PS tethered chains are repulsed from the substrate surface [40]. The other reason is associated with the quality of applied solvent at growth condition. Though at adopted condition, amyl acetate is a very good solvent for PS blocks, it is a partially poor solvent for PMMA blocks [39,42-44]. That is why we were able to design the matrix-dispersed surface morphologies during growth of single crystals from mentioned diblock copolymer chains. It could be named as a sort of *single crystal surface patterning*. In this leopard skin-like pattern, patches are made of PMMA brushes, which are reluctant to abandon the PEG substrate surface, and skin itself is formed of stretched PS tethered chains. We used bulk atactic densities of PMMA and PS to do our calculations [44,45]. It is noteworthy that the constructed mixed-brush surface morphologies were not in request of any selective solvent to be detected. Regarding different hardnesses of the PMMA and PS amorphous blocks [38,46,47], detection of phase regions on the single crystal substrate was possible.

Fabrication of epitaxial nanostructures from various amorphous-crystalline diblock copolymers including PEG-*b*-PS, PEG-*b*-PMMA, and homo-PEG chains was the last issue tackled in this work. In addition to having chemical and geometric recognition applications [42], in this work the channel-wire arrays have been employed to verify the corresponding thickness of substrate in different phase regions of single crystals with mixed-brush surface morphologies. To grow the epitaxial structures inevitably, the PEG_{5000}-*b*-PS_{4600} single crystals, which had the least hindrance against the growth of subsequent layers, were used as innermost crystals. Consequently, through growth of homo-PEG layer we could obtain the sublayer thickness of region covered by PS ($\bar{M}_n$ = 4600 g/mol) tethered chains using the conjunction thickness between the PEG-*b*-PS and homo-PEG single crystal. Afterward, the PEG-*b*-PMMA and homo-PEG layers were grown, respectively to acquire the substrate thickness of surface areas covered by the PMMA grafted chains via the corresponding conjunction thickness.

Experimental

Synthesis

The bromo-capped PEG macroinitiator (PEG-Br) (MI) was synthesized and purified according to the literature [48,49]. The diblock copolymers of PEG-*b*-PS and PEG-*b*-PMMA including various molecular weights of PS and PMMA blocks were synthesized via solution polymerization in chlorobenzene (CB, Merck, > 99%) and with the agent ratio of ([styrene (St)]$_0$/[MI]$_0$/[CuBr]$_0$/[bipy]$_0$ /[CB]$_0$) = 240/1/1/3/66) and ([methyl methacrylate (MMA)]$_0$/[MI]$_0$/[CuCl]$_0$[$CuCl_2$]$_0$/[bipy]$_0$/[CB]$_0$) = 177/1/1/0.07/3/ 375) by ATRP. The reaction temperatures for St and MMA polymerization were 110 and 65 °C, respectively. Due to higher reactivity of MMA in comparison with St [50,51], $CuCl_2$ (Merck, > 98%) was used as deactivator for better controlling of polymerization [52]. Related explanations of synthesis procedures are described elsewhere [53,54]. Characteristic of ATRP, the GPC traces (Figure S1) were narrow, symmetric, mono-modal, and moved with increasing conversion towards lower elution volume, i.e., elevated molecular weights. The molecular characterization data of diblock copolymers used in this work are reported in Table 1.

Table 1. Molecular characteristics of the synthesized samples ($\bar{M}_n^{AMORPH}$refers to the number-average molecular weight of PS or PMMA blocks)

Sample	$\bar{M}_n$(g/mol)	$\bar{M}_n^{PEG}$(g/mol)	$\bar{M}_n^{AMORPH}$(g/mol)	$\bar{M}_w/\bar{M}_n$
Homo-PEG_{5000}	5,000	5,000	0	1.06
PEG_{5000}-*b*-PS_{4600}	9,600	5,000	4,600	1.13
PEG_{5000}-*b*-PS_{10000}	15,000	5,000	10,000	1.15
PEG_{5000}-*b*-PS_{14800}	19,800	5,000	14,800	1.16
PEG_{5000}-*b*-$PMMA_{8700}$	13,700	5,000	8,700	1.19
PEG_{5000}-*b*-$PMMA_{13100}$	18,100	5,000	13,100	1.21
PEG_{5000}-*b*-$PMMA_{17100}$	22,100	5,000	17,100	1.20

Single crystal growth

The details of self-seeding technique used for growing of PEG-*b*-PS diblock copolymer single crystals have been described elsewhere [55,56]. Here, we have adopted this approach to grow the single crystals with mixed-brush surface morphologies.

Solution crystallization was carried out with a dilute concentration of 0.018 wt% (wt/wt of PEG-*b*-PS/PEG-*b*-PMMA was 50/50) in amyl acetate (Merck, > 98%). The sample was put into a cell tube containing solvent. Then cell tube was sealed, and heated to above the dissolution temperature of the sample in the solvent (T_d = 65 °C) in a temperature-controllable oil bath and kept for about 10-15 minutes to erase the thermal history, and to reach a homogeneous solution as well. Then, the cell tube was transferred to another bath at present −10 °C lasting 5-6 h for fast crystallization, and then immersed into a given self-seeding temperature oil bath (T_s= 41 °C for all samples), and kept for 20 min. The cell tube in question was then quickly transferred into a desired crystallization temperature isothermal oil bath and maintained for 2-3 days.

To fabricate the epitaxial structures, first, the single crystals of diblock copolymers at solute concentration of 0.009 wt% were grown similarly. After complete crystallization of the diblock copolymers (or homopolymers), a few drops of the sample containing the copolymer (or homopolymer) single-crystal seeds were added into the homogeneous solution of homopolymer (or copolymer) which had been kept in the same crystallization oil bath. In experiments of epitaxial growth, the exact amount of transferred seeds was not clear. However, it was obvious that the population was different from one sample to another. The various lateral sizes of channels proved our claim (the wider channel the lower transferred population of seeds). Nevertheless, volume wise, in each stage we transferred 0.7 ml of solution containing seeds. The homogeneous homopolymer (or copolymer) solution was prepared by heating the mixture of homopolymer (or copolymer) and solvent up to 65 °C for 20 min. The solution was then quickly switched into the crystallization oil bath (at a preset T_c) for about 10 min to reach the thermal equilibrium before adding the diblock (or homopolymer) single crystal seeds. During this period, no crystals were found. The homopolymer (or copolymer) crystals then grew on the diblock copolymer (or homopolymer) single-crystal seeds to form composite single crystals.

Results and discussion

It has been investigated that PEG-*b*-PS diblock copolymers can crystallize in dilute solutions to grow the single crystals having a PEG block single crystal as the middle layer and the PS block layers at the top and bottom of the basal surfaces to fabricate a sandwich structure [42,55,56]. In the present work, we have grown mixed-brush single crystals with matrix-dispersed surface morphology and square shape. The strongest diffraction spots in Figure 1(b) are ascribed to the (120), ($\bar{1}$20), (1$\bar{2}$0) and ($\bar{1}\bar{2}$0) planes (identical to the homo-PEG [57-60] as well as homo-brush single crystals [39,42,43,60]), showing that the PEG chain direction in the crystal is parallel to the surface normal. Figure 1depicts the transmission electron microscope (TEM) bright image of a PEG_{5000}-*b*-PS_{4600}/PEG_{5000}-*b*-$PMMA_{8700}$ single crystal grown at T_c= 28 °C (a) and related electron diffraction (ED) pattern (b). Some darker spots in TEM image illustrate the PMMA-dispersed patches with different crystalline substrate thickness in comparison to respective substrate thickness of PS-matrix. Considering Figure 1(c) which shows scanning transmission electron microscopy (STEM) image of PEG_{5000}-*b*-PS_{4600}/PEG_{5000}-*b*-$PMMA_{13100}$single crystal grown at T_c= 30 °C, one can see that all single crystals are identical and resemble each other apparently; it is known that mentioned uniformity is the feature of self-seeding method [37,40].

Detection of various phase regions in mixed-brush morphologies

As mentioned previously, the mixed tethered chains on the substrate comprise two different phase areas, which fall into matrix and dispersed phases. Figure 1(a) and (d) are representative of TEM bright image of PEG_{5000}-*b*-PS_{4600}/PEG_{5000}-*b*-$PMMA_{8700}$ single crystal grown at T_c = 28 °C and AFM height image of PEG_{5000}-*b*-PS_{10000}/PEG_{5000}-*b*-$PMMA_{13100}$single crystal grown at T_c = 23 °C, respectively, which clearly indicate the mentioned morphology. Here, without any requirement to the solvent treatments we were able to distinguish the various matrix and dispersed phase regions. The ultimate ratio of PMMA-covered patches to PS-covered matrix region is less than 50/50 (primary ratio used to grow single crystals). This is to say that in growth systems there have been some single crystals covered only by PMMA brushes. Hence, the excess of PEG-*b*-PMMA diblock copolymers construct such homo-brush single crystals.

Such a distribution for polymer mixed-brushes could be associated with two main reasons. First is for the different conformations of PS and PMMA amorphous blocks in amyl acetate. The applied solvent at growth condition (23-32 °C) could be considered a partially poor solvent for PMMA block, whereas it is a very good solvent for PS one [42-44]. Therefore, the PS chains are more extended in comparison to the PMMA ones. The mentioned conformation for PS blocks may cause PEG-*b*-PS chains to be included into the single crystal structure more conveniently. That is why the surface areas comprising the PS tethered chains construct the matrix phase. Second, as stated previously, the interaction of substrate surface with PMMA and PS grafted chains are of the kind of attraction and repulsion, respectively. Hence, the grafted PMMA chains tend to be attracted to the substrate surface and, subsequently, increase the segmental density in the vicinity of it; on the contrary, the PS ones like to be repulsed from the surface and reach to the more extended conformations. The PMMA chains possess somewhat packed pancake shape conformation; so, their hindrance against the chains with the same blocks is significantly high. Any way, it may be declared that due to compatibility of PMMA chains with PEG crystalline blocks [61] and their more coily conformations, the tethered PS chains treat them like homo-PEG chains, so the chains in question are capable to enter into the single crystal structure. Besides, for high hindrance of PMMA grafted chains, the phase regions constructed with them could only contribute to small spread patches.

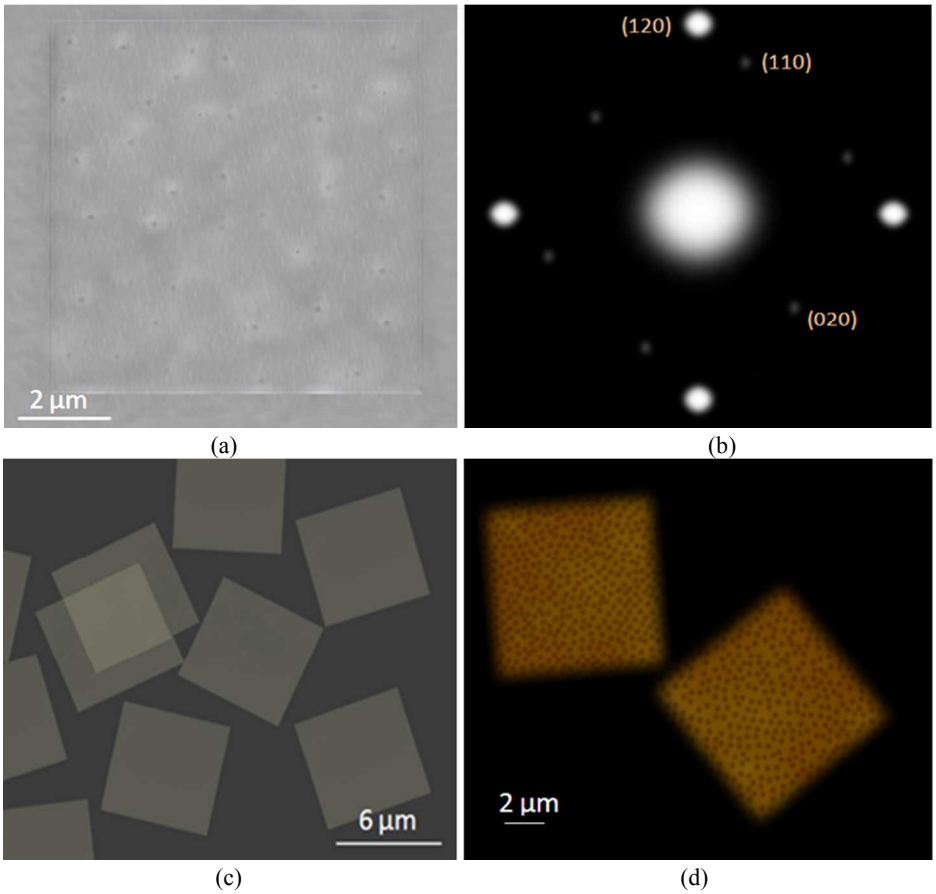

Figure 1. TEM bright image of PEG_{5000}-*b*-PS_{4600}/PEG_{5000}-*b*-$PMMA_{8700}$ single crystal grown at T_c = 28 °C (a) accompanied by ED pattern (b); STEM image of PEG_{5000}-*b*-PS_{4600}/PEG_{5000}-*b*-$PMMA_{13100}$ single crystal grown at T_c = 30 °C (c); AFM height image of PEG_{5000}-*b*-PS_{10000}/PEG_{5000}-*b*-$PMMA_{13100}$ single crystal grown at T_c = 23 °C (d). The weight ratio of PEG-*b*-PS/PEG-*b*-PMMA diblock copolymers was 50/50 for cocrystallization of all samples.

From macroscopic view point, PMMA is harder than PS on the basis of Rockwell hardness which are M80-M105 and M65-M85 for PMMA and PS, in respect [38,46]. Microscopy wise, the depth of a static indentation for an AFM tip penetrating into PS regions is approximately 5 nm while a tip penetrating into PMMA domains is less than 1 nm [38,47]. Therefore, the opaque phases are PMMA-disperses.

In some samples, the height variance between matrix and disperse phases was very low. Hence, the hardness variances could be considered a determinant parameter in detection. Figure 2(a) depicts the PEG_{5000}-*b*-PS_{4600}/PEG_{5000}-*b*-$PMMA_{17100}$ mixed-brush morphology constructed at T_c = 23 °C. The height variance between matrix and disperse phase regions is equal to 1.9 nm. Here, the PMMA-dispersed domains are much blur in comparison with matrix phase constructed with PS grafted chains on the substrate. Similarly, in Figure 2(b) the corresponding morphology of PEG_{5000}-*b*-PS_{10000}/PEG_{5000}-*b*-$PMMA_{13100}$ mixed-brush single crystal constructed at T_c = 30 °C has been shown, in which the height variance is 5.7 nm. With increasing the height variance, the clarity of images rises. Figure 2(c) is related to the surface morphology of PEG_{5000}-*b*-PS_{14800}/PEG_{5000}-*b*-$PMMA_{17100}$ mixed-brush single crystal in which the height variance is equal to 6.7 nm. It seems that the last morphology, due to its elevated height variance between matrix and dispersed phases, has higher resolution.

Journal Name

RSCPublishing

ARTICLE

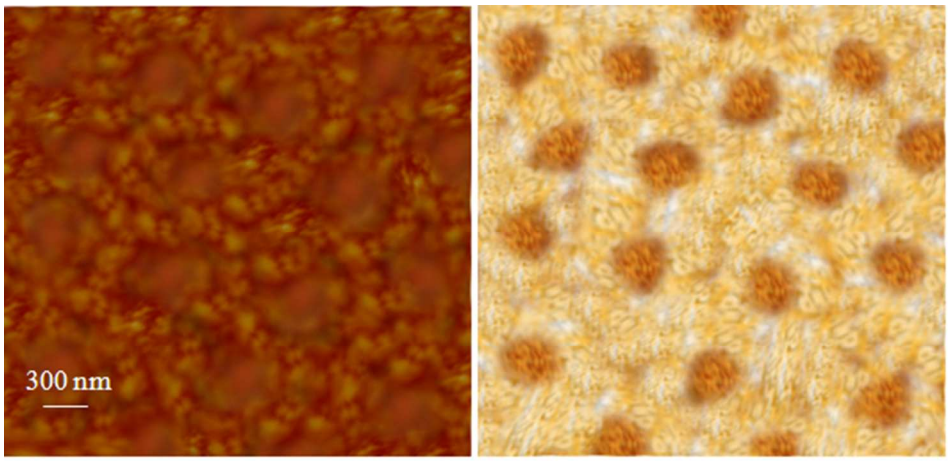

(a)

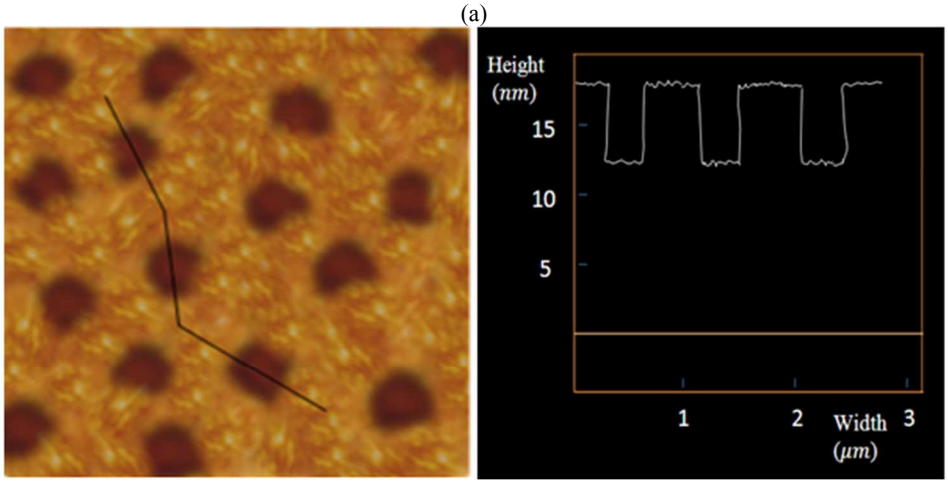

(b)

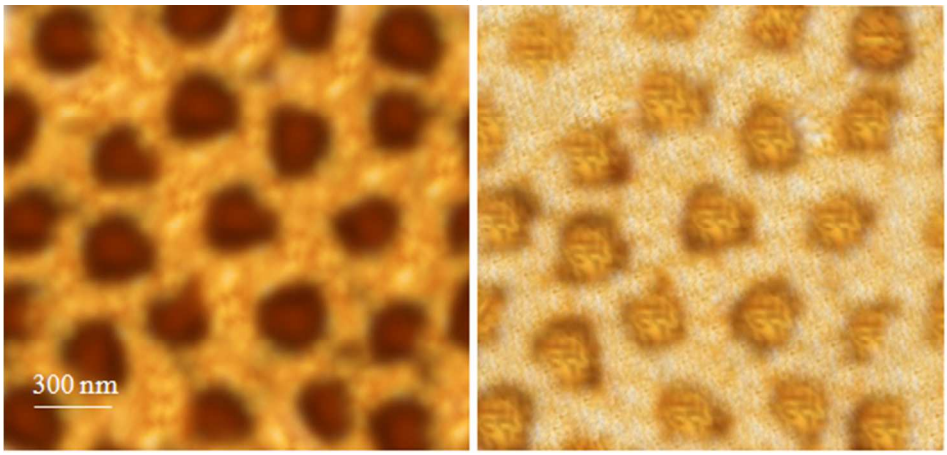

(c)

Figure 2. AFM NanoscopeIII images of mixed-brush single crystals. Surface morphology of PEG_{5000}-*b*-PS_{4600}/PEG_{5000}-*b*-$PMMA_{17100}$ (grown at T_c = 23 °C), left: height image (the maximum z-scale is 5 nm), height variance: 1.9 nm, domain size: 302 nm, right: phase image (the maximum z-scale is 5°) (a); surface morphology of PEG_{5000}-*b*-PS_{10000}/PEG_{5000}-*b*-$PMMA_{13100}$ (grown at T_c = 30 °C), left: height image (the

maximum z-scale is 5 nm), height variance: 5.7 nm, domain size: 314 nm, right: height profile (b); surface morphology of PEG_{5000}-*b*-PS_{14800}/PEG_{5000}-*b*-$PMMA_{17100}$ (grown at T_c = 30 °C), left: height image (the maximum z-scale is 5 nm), height variance: 6.7 nm, domain size: 287 nm, right: phase image (the maximum z-scale is 5°) (c). The weight ratio of PEG-*b*-PS/PEG-*b*-PMMA diblock copolymers was 50/50 for cocrystallization of all samples.

The effect of PS block molecular weight on the thickness, tethering density and the PMMA dispersed domain size

In mixed-brushes, like homo-brush single crystals, via enhancement of amorphous block molecular weight, the total thickness due to increase of amorphous layer height increases; because the brushes want to overcome the overlapping. However, the crystalline substrate thickness decreases.

The escalation of osmotic pressure (a pressure exerted by a tethered chain on the surface of single crystal substrate to provide its required surface area to be expanded) resulting from need of amorphous chains to provide their coverage surface area will cause the substrate to decrease its thickness. That is why, the folding number of crystalline chains is raised and, consequently, the tethered chains on the substrate surface will get distance from each other [62-66]. The explanations in question for alteration of PS molecular weights are reported in Tables S1 and Figure 3.

By increasing M_n^{PS} while PMMA features are kept constant, the clarity of images will be intensified, because height variance between PS-matrix and PMMA-dispersed phase regions is on the rise. These have been graphically depicted in Figure 2(c) and Figure 3(a). Here, the colour variance is an important to identify the different phase regions. Besides, it is notable that the features of each phase region are only effective on its own thickness as well as tethering density. Keeping all other influencing parameters at a certain condition and changing the molecular weight of amorphous block of PS as a type, only the overall thickness and tethering density of PS-covered areas undergo the related alterations. Mentioned relation satisfies the condition of corresponding PMMA systems as well (next section). As an instance, at T_c = 23 °C, where the molecular weight of PS reached from 10000 to 14800 g/mol, whereas that of PMMA was constant (= 17100 g/mol), the total thickness varied from 16.4 to 18.4 nm; the respective tethering densities changed from 0.37 to 0.30 nm^{-2} (Table S1); here, one can behold that the thickness (= 12.3 nm) and tethering density (= 0.20 nm^{-2}) of PMMA regions have remained constant. These are graphically illustrated in Figure 3(a) and tabulated in Table S1. The thickness and tethering density of the PMMA domains do not change via molecular weight of PS brushes. For example, where the molecular weight of PS reached from 4600 to 10000 g/mol while that of PMMA was fixed in 13100 g/mol at T_c = 23 °C, the thickness and tethering density of PMMA domains were equal to 11.2 nm and 0.22 nm^{-2}, respectively (Table S1).

The domain size is defined through calculating the average of the longest and shortest lines, which connect two points on the perimeter of each domain. Percentage speaking, the somehow insignificant tolerances from the respective average disperse domain size are reported in all data Tables (S1, S2 and, S3). With increasing the PS molecular weight, the hindrance against the absorption of PEG-*b*-PMMA chains into the single crystal structure increases. So, the PMMA-disperses size reduces. It could be associated with this fact that PS's hindrance against the PMMA chains will be intensified. Table S1 represents the trend of PMMA dispersed domain size changes via variation of PS amorphous block molecular weights (where the molecular weight of PMMA blocks are constant) at completely the same growth condition (self-seeding, crystallization temperatures and solvent quality). As an instance at T_c = 23 °C, raising the molecular weight of PS from 4600 to 10000 and finally to 14800 g/mol while that of PMMA was fixed at 17100 g/mol, the domain size of dispersed phase decreased from 302 to 295 and 286 nm gradually. This trend is shown in Figure 3(b). The tethering density (σ) and crystalline substrate thickness (d_{CRYST}) can be determined from Equation (1) and (2), respectively [39,42,43].

$$\sigma = \frac{1}{S} = \frac{1}{\frac{2M_n^{CRYST}}{N_A \rho_{CRYST} d_{CRYST}}} = \frac{N_A \rho_{CRYST} d_{CRYST}}{2M_n^{CRYST}} \quad (1)$$

$$d_{CRYST} = d^{total} \times \frac{M_n^{CRYST}/\rho_{CRYST}}{M_n^{CRYST}/\rho_{CRYST} + M_n^{AM}/\rho_{AM}} \quad (2)$$

where σ, N_A, ρ_{CRYST},d_{CRYST},M_n^{CRYST}, d^{total}, M_n^{AM}, and ρ_{AM}stand for the tethering density, the Avogadro number, crystalline PEG density (is equal to 1.239 g/cm^3 at room temperature) [45], PEG substrate thickness which is given in Equation(2), the molecular weight of PEG which is constant and equal to 5000 g/cm^3 for all samples, the overall thickness, the molecular weight of amorphous blocks, the density of amorphous blocks (1.19 g/cm^3 [44] for PMMA and 1.05 g/cm^3 [45] for PS), respectively. These are reported for atactic PS and PMMA. When styrene polymerization is initiated with free radicals, the chains will get atactic stereoregularity [67]. In this work, we adopted a controlled free radical polymerization with atom transfer feature (ATRP). Therefore, there will be no difference in the stereoregularity.

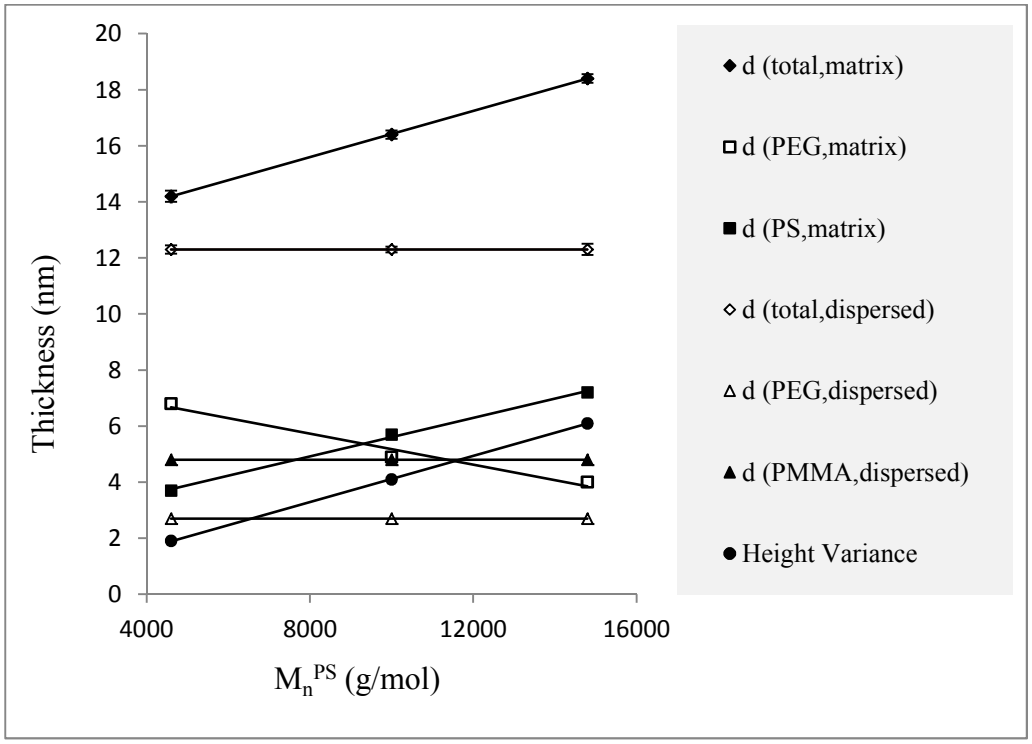

(a)

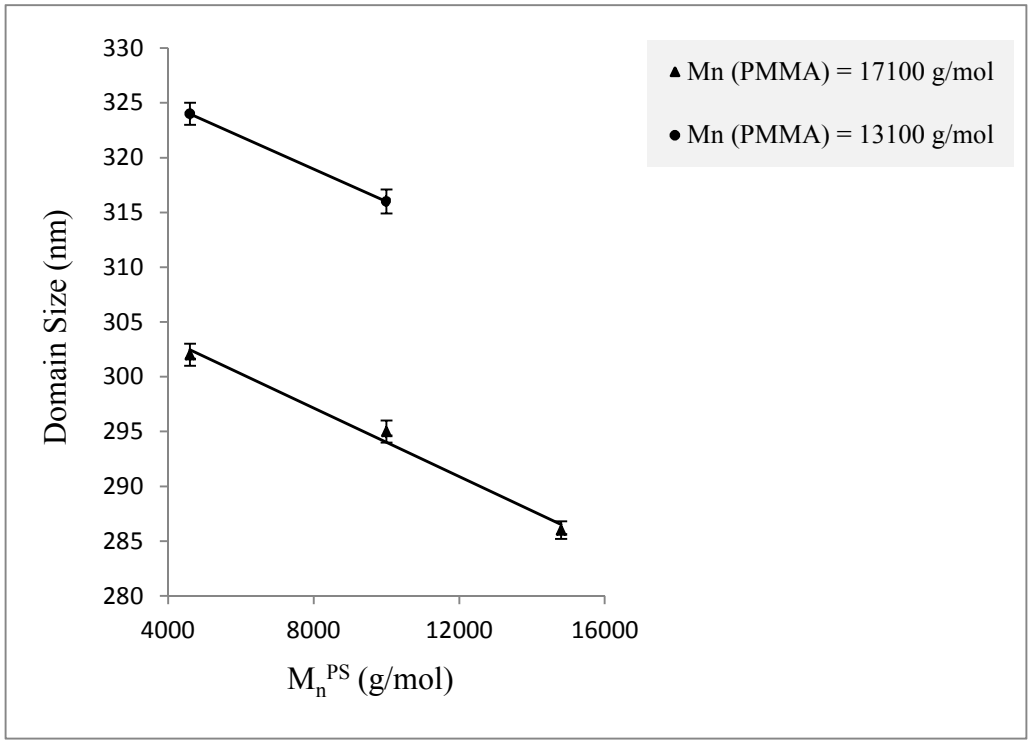

(b)

Figure 3. The effect of PS block molecular weight on the total, substrate and amorphous brushes thicknesses of single crystals grown at T_c = 23 °C where M_n^{PMMA} = 17100 g/mol and M_n^{PS} changed from 4600 to 10000 and, subsequently, to 14600 g/mol (a); the effect of PS block molecular weight on the average domain size of PMMA-disperses at T_c = 23 °C (b).

Journal Name RSCPublishing

ARTICLE

The influence of PMMA block molecular weight on the thickness, tethering density and the PMMA dispersed domain size

PMMA molecular weight enhancement, where all properties of PS tethered chains are fixed, is to the detriment of height images clarity; because the height variance is on the fall. This is shown graphically in Figure 2(a) and Figure 4(a). Therefore, the opaqueness and transparency of different phase regions, which belong to PMMA-dispersed and PS-matrix phases, respectively, is more helpful. At T_c = 23 °C, where the molecular weight of PMMA reached from 8700 to 13100 g/mol, while that of PS was constant (= 4600 g/mol), the total thickness varied from 10.0 to 11.2 nm. The corresponding tethering densities changed from 0.26 to 0.22 nm^{-2}, whereas the thickness (~ 14.2 nm) and tethering density (~ 0.51 nm^{-2}) of PS regions remained constant. This trend is represented in Figure 4(a) as well as Table S2. Moreover, where the molecular weights of PS and PMMA blocks changed somewhat similarly, alteration of thickness and tethering density in PS region was more pronounced than that of PMMA-covered patches; because the respective osmotic pressure among PS chains is less than that of PMMA ones.

Whit increasing M_n^{PMMA} while all other parameters, especially PS block molecular weight, were constant the domain sizes of PMMA dispersed patches decreased. This trend could be attributed to the increase of PMMA tethered chains hindrance. Raising M_n^{PMMA}, the tethered chains on the substrate surface will be in dire need of more expanded area to cover. It not only affects the PMMA brushes conformation but also reduces the probability of PEG-*b*-PMMA chains presence in the single crystal structure. Table S2 shows the trend of M_n^{PMMA} variation (for constant M_n^{PS}). As an instance, increasing the molecular weight of PMMA block from 8700 to 13100 and, subsequently, to 17100 g/mol, where M_n^{PS} was equal to 4600 g/mol at T_c = 23 °C, the respective domain sizes of dispersed phase reduced from 350 to 324 and 302 nm, respectively (Figure 4(b)).

An interesting point is that the heights of the PMMA tethered chains are less than the corresponding heights of PS brushes. This trend is satisfied even when the molecular weight of PMMA brushes is considerably higher than that of PS ones (17100 vs. 4600 g/mol). As described, it could be associated with the solvent quality as well as interactions with the substrate surface. In PEG_{5000}-*b*-PS_{4600}/PEG_{5000}-*b*-$PMMA_{17100}$ mixed-brush single crystals at T_c = 23 °C, despite having higher molecular weight, the height of PMMA brushes was lower (12.3 vs. 14.2 nm).

The effect of PMMA block molecular weight on the dispersed domain size deduction was more intensified. As an instance, at T_c= 23 °C with changing the molecular weight of PS block from 4600 to 10000 g/mol while that of PMMA was fixed at 13100 g/mol, the domain size of dispersed phase decreased from 324 to 316 nm (Figure 3(b)). In spite of this smooth reducing trend, at the same T_c via soaring of M_n^{PMMA} from 8700 to 13100 g/mol while that of PS was constant (= 4600 g/mol), the domain sizes of PMMA dispersed phase diminished from 350 to 324 nm (Figure 4(b)). In the latter sample, even though the hindrance of PS chains was minimum (M_n^{PS} = 4600 g/mol), the dispersed domain size reduction with escalating the PMMA molecular weight has been conspicuous, and it could be attributed to the prevalent influence of conformation of PMMA tethered chains. This comparison can be drawn from the slope of graphs of domain size vs. amorphous block molecular weight (Figure 3(b) and Figure 4(b)).

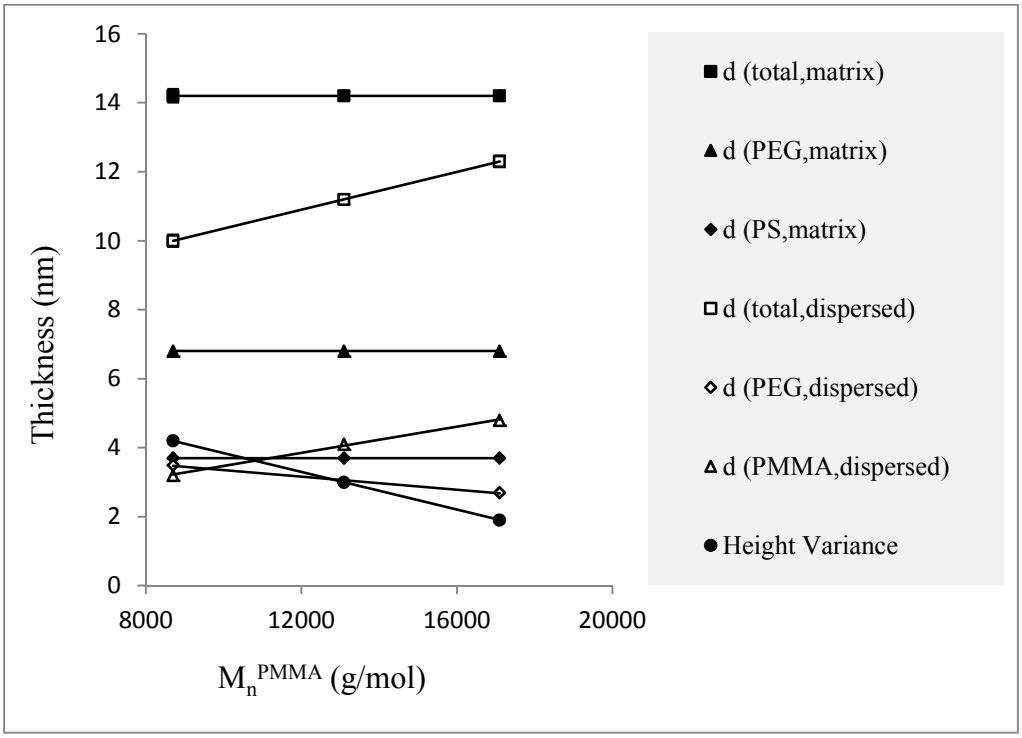

(a)

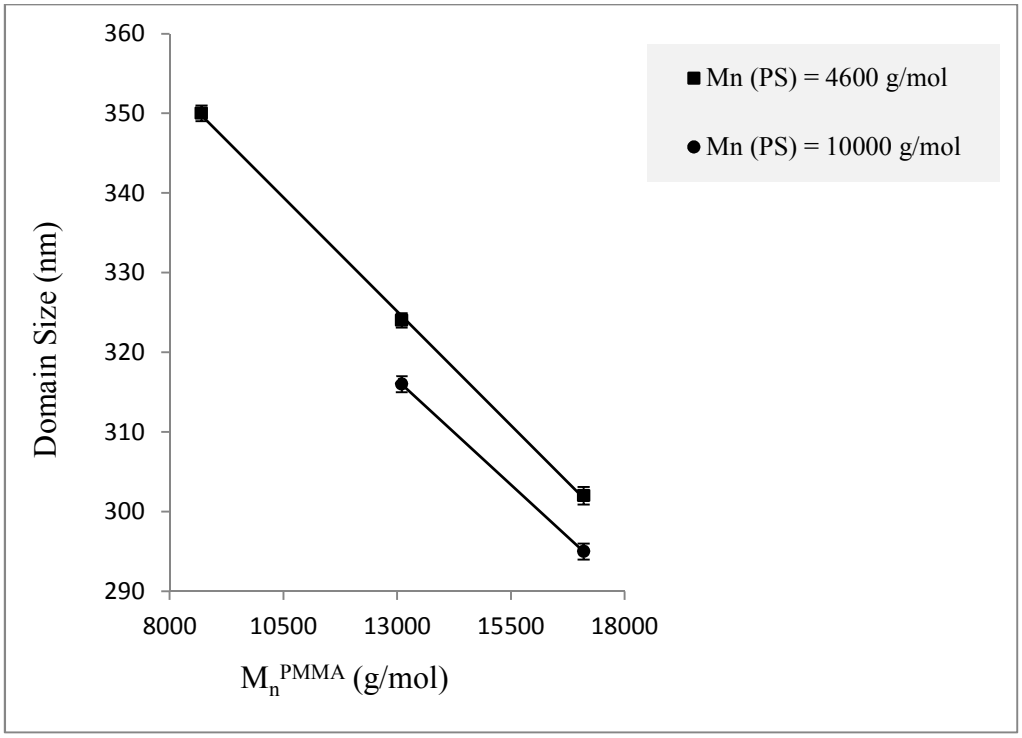

(b)

Figure 4.The effect of PMMA block molecular weight on the total, substrate and amorphous brushes thicknesses of single crystals grown at T_c= 23 °C where M_n^{PS} = 4600 g/mol and M_n^{PMMA} changed from 8700 to 13100 and, subsequently, to 17100 g/mol (a); the effect of PMMA block molecular weight on the average domain size of PMMA-disperses at T_c= 23 °C (b).

Journal Name RSCPublishing

ARTICLE

The influence of crystallization temperature on the single crystal thickness and tethering density of mixed-brushes

In polymer mixed-brushes as well as homo-brushes, via increasing the crystallization temperature, the total height and substrate thickness of single crystals in both matrix and dispersed phases increased. This enhancement could lie in the substrate thickness increase and amorphous grafted brushes thickening as well. Keeping the crystallization temperature (T_c) at a constant point, one is able to fix the thickness of single crystal substrate (d_{CRYST}), because it is a function of undercooling degree (Equation (3) [68-70]).

$$d_{\mathrm{CRYST}} \propto \frac{1}{\Delta T_{\mathrm{undercooling}}} = \frac{1}{T_d - T_c} \quad (3)$$

This equation indicates that the effective parameters on $\Delta T_{undercooling}$ are dissolution temperature (T_d) and T_c. Besides, the thickness enhancement of crystalline substrate could be related to the tendency of PEG chains to reach to the more stretched state (to reduce the free energy via T_c increase [59]). With increasing the crystalline substrate thickness and approaching the tethered chains to each other, the number of tethered chains per surface area rises. The trend of thicknesses and tethering densities related to the PMMA and PS phase regions for mixed-brush surface morphologies are reported in Table S3. By crystallization temperature elevation, both substrate and amorphous layer heights in PS-matrix, increase more than those in PMMA-disperses. The higher increase of crystalline substrate beneath the PS tethered chains is due to lower osmotic pressure exerted with PS chains in comparison to PMMA ones. To prove that the osmotic pressure of PS tethered chains is less than that of PMMA grafted ones, we bring two different systems into consideration. One of them comprises the PEG-*b*-PS diblock copolymers with the highest molecular weight of PS in amyl acetate which is a very good solvent for PS, whereas the other one includes PEG-*b*-PMMA diblock copolymers with the least molecular weight of PMMA in partially poor solvent. Regarding the gyration radii of PS with $\bar{M}_n$ = 7700 g/mol in a very good solvent (= 3.7 nm) [37] and PMMA with $\bar{M}_n$ = 7800 g/mol in a nearly good solvent (= 3.4 nm) [40], and comparing these data with our growth system, we could reach to some results. In this work, applied solvent, amyl acetate, is partially poor for PMMA, and the corresponding molecular weight of its block is significantly less than that of PS block. Therefore, the gyration radius of PS is higher than respective radius of PMMA. Conducting experiments with more scrutiny, it could be said that at completely the same growth condition, the substrate thickness of PMMA covered single crystal is considerably less than corresponding thickness of PS covered substrate. Therefore, the impact of attractive interaction between PMMA chains and single crystal substrate is a dominant parameter on its substrate thickness. We speculate that the mentioned interaction could in turn have the most significant effect on the exerted osmotic pressure of chains and substrate thickness as well. As it mentioned previously, amorphous block molecular weight alteration is effective only on the thickness and tethering density, which belong to that region. Therefore, we are able to make a comparison between the thickness of PS region in PEG_{5000}-*b*-PS_{14800}/PEG_{5000}-*b*-$PMMA_{17100}$and that of PMMA region in PEG_{5000}-*b*-PS_{4600}/PEG_{5000}-*b*-$PMMA_{8700}$ mixed-brush single crystals at T_c= 23 °C. If we want to exemplify the presented explanations, we could say the thickness of substrate underneath the PS ($\bar{M}_n$ = 14800 g/mol) brushes is 4.0 nm, whereas that of PMMA ($\bar{M}_n$ = 8700 g/mol) ones is equal to 3.5 nm.

Actually, two main reasons could be presented for significant enhancement of PS amorphous layer height. First, the increase of substrate thickness in PS growth systems is more than that of PMMA ones. Hence, the tethering density will increase in PS single crystals conspicuously in comparison to PMMA ones. So, the steric repulsion between PS tethered chains highly gets raised and, consequently, they tend to reach to more stretched conformation. For a more complete coverage of this subject, due to repulsive interaction of PS grafted chains with the substrate surface, they are allowed to be freely stretched, and disapproach from the surface. If we put together all mentioned effective parameters, we will be able to conclude that via enhancement of crystallization temperature, the variance between PMMA and PS phase regions gets larger amounts (Figure 5(a)) and, consequently, the clarity of height images to distinguish the various phases, increases. As an instance, for mixed-brush morphologies created from PEG_{5000}-*b*-PS_{10000}/PEG_{5000}-*b*-$PMMA_{13100}$, through changing the crystallization temperature from 23 to 30 °C, the PS phase thickness reached from 16.4 to 18.2 nm; whereas the thickness of PMMA dispersed phase increased from 11.2 to 12.5 nm, respectively (Table S3).Another example is graphically illustrated in Figure 5(a) for PEG_{5000}-*b*-PS_{4600}/PEG_{5000}-*b*-$PMMA_{8700}$ single crystal.

Considering the reported data in Table S3, the domain sizes of PMMA-disperses in PS-matrix do not change via crystallization temperature alteration, and it could be related to the constancy of effective parameters on the disperse domain sizes (i.e., molecular weight of PS and PMMA amorphous blocks).

For example, in mixed-brush morphologies created from PEG_{5000}-*b*-PS_{14800}/PEG_{5000}-*b*-$PMMA_{17100}$, through changing the crystallization temperature from 23 to 30 °C, the dispersed domain size was fixed in to some extent 286 nm (Figure 5(b)). This trend satisfied the conditions for other samples as well.

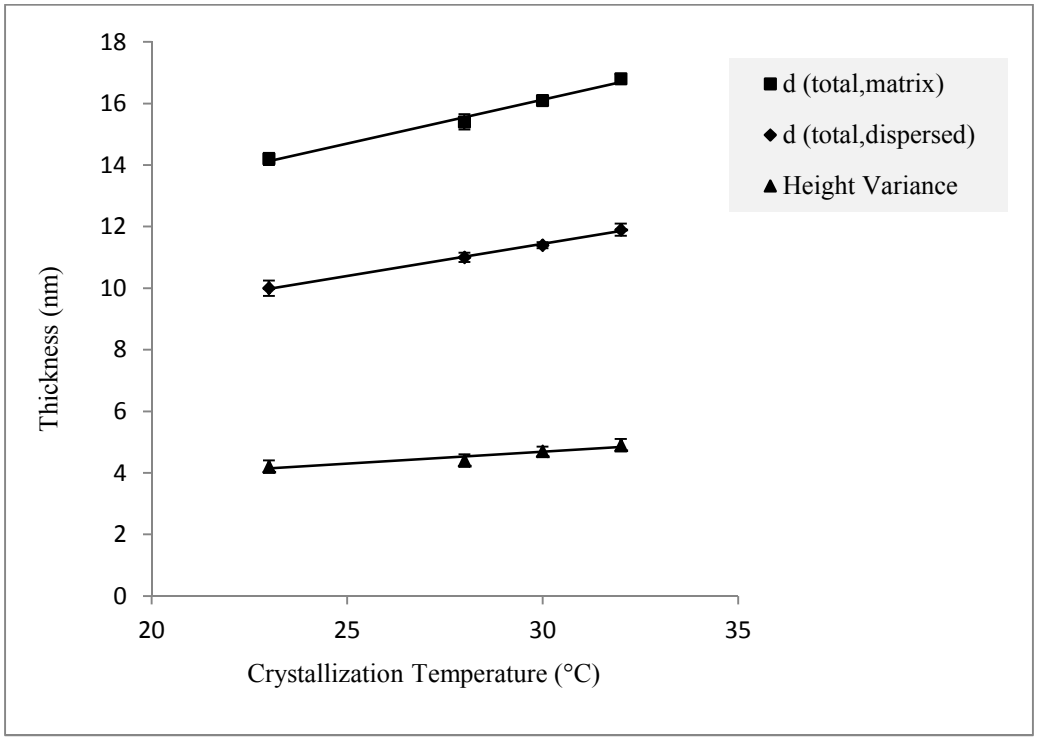

(a)

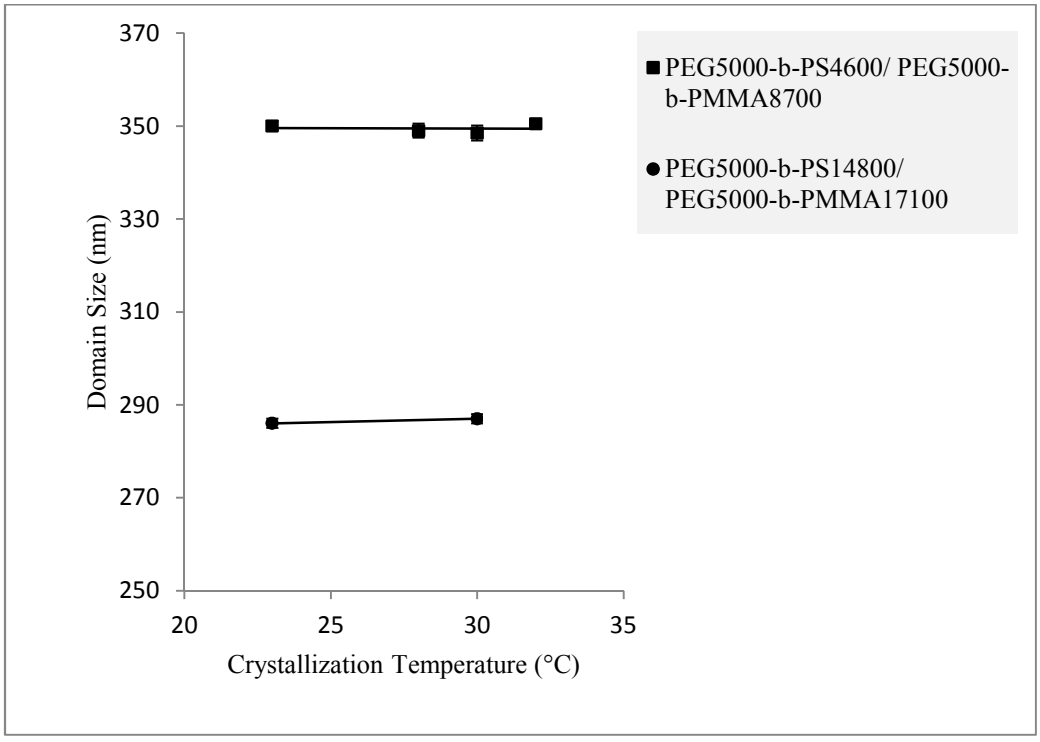

(b)

Figure 5. The effect of crystallization temperature on the total thicknesses of PS-matrix and PMMA-dispersed phase regions of PEG_{5000}-*b*-PS_{4600}/PEG_{5000}-*b*-$PMMA_{8700}$ single crystal (a); the effect of crystallization temperature on the average domain size of PMMA-disperses (b).

Adopting the polymer epitaxial structures to verify the crystalline substrate thickness determined in mixed-brush single crystals

We grew single crystals of PEG_{5000}-*b*-PS_{4600} and used them as the seeds for further growth of second layer including homo-PEG_{5000}. Subsequently, this procedure was repeated to form a nanostructure

including outer layers of PEG_{5000}-*b*-$PMMA_{8700}$ (other molecular weights of PMMA consisting 13100 and 17100 g/mol were applied to create the corresponding layers in the remaining samples) and homo-PEG_{5000} as well. The material of crystalline block and homopolymer was the same; so, the epitaxial growth could thus occur with the identical growth fronts. At the conjunction between diblock copolymer and homopolymer single crystals, the thickness has to be confined to the same thickness, which is provided by previously presented growth fronts. The crystalline substrate thickness at the conjunction of diblock copolymer and homopolymer is equal to that of diblock copolymer single crystal. However, the thermodynamic metastable thickness of these two crystals will not be remained the same. As the crystal grows away from the seed, the thermodynamic thickness will be reached, which is larger than primary substrate thickness definitely. Therefore, the measurement of thickness at the conjunction of copolymer and homopolymer crystals could provide an accurate determination for the substrate thickness of copolymer single crystals [39-42].

Regarding the conjunction thickness between the copolymer and homopolymer crystals, which is achievable from the height profile, we were capable to verify the calculated crystalline substrate thickness in single crystals with matrix-dispersed surface morphology. While depositing the crystals onto a hard silicon wafer surface during AFM analyses, the homo-PEG single crystals may slip down to the silicon surface for the gravity effect, as it can be seen in height profile of Figure 6(b). Here, the thicknesses achieved at the conjunctions of the copolymer seeds is a direct measure of the d^{PEG}. The calculated thicknesses of the PMMA and the PS phases in mixed-brush single crystals are highly adapted with the achieved thicknesses from respective layers of epitaxial structures. As an instance, considering data of Table S3 and Figure 6, related to the height image of surface morphology and height profile (a) and height image and height profile of corresponding epitaxial structure (b) respectively, it could be understood that in mixed-brush single crystal of PEG_{5000}-*b*-PS_{4600}/PEG_{5000}-*b*-$PMMA_{8700}$, the calculated thicknesses of the PS and PMMA regions are equal to 7.7 and 4.0 nm, respectively. It is interesting that the corresponding achieved substrate thicknesses from epitaxial structure for PS and PMMA covered areas are the same (i.e., 7.7 and 4.0 nm).

Moreover, this consistency indicates that our primary hypotheses for PS, PMMA and PEG (here we used the bulk density of atactic PS and PMMA blocks for their respective tethered chains; besides, we ignored the bulk density of amorphous PEG) are completely true.

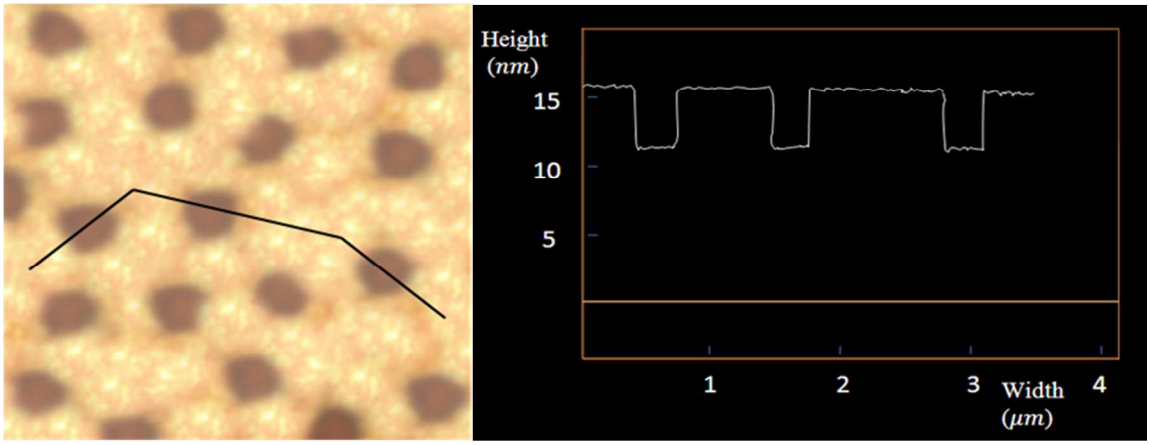

(a)

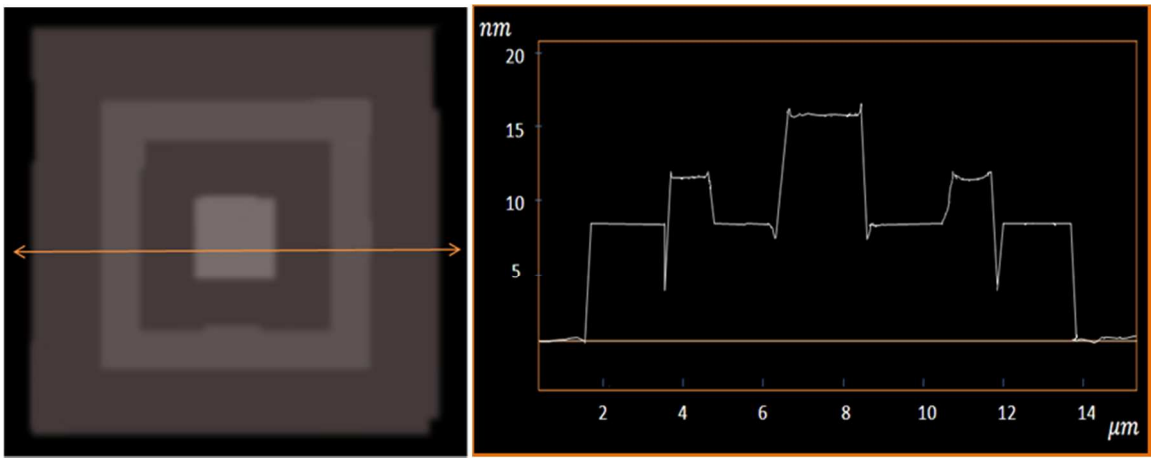

(b)

Figure 6. AFM NanoscopeIII image of mixed-brush single crystals. Surface Morphology of PEG_{5000}-*b*-PS_{4600}/PEG_{5000}-*b*-$PMMA_{8700}$ at T_c = 30 °C, left: height variance: 4.7 nm, domain size: 348 nm; right: height profile. The weight ratio of PEG-*b*-PS/PEG-*b*-PMMA diblock copolymers was 50/50 for cocrystallization (a); left: epitaxial structure of PEG_{5000}-*b*-PS_{4600} ⇒ homo-PEG_{5000} ⇒ PEG_{5000}-*b*-$PMMA_{8700}$ ⇒ homo-PEG_{5000} at T_c = 30 °C, right: height profile (b).

Conclusions

We could prepare single crystals with the matrix (PS)-dispersed (PMMA) surface morphologies. Various conformations of PMMA and PS chains, could in turn be a reasonable cause for higher probability of crystalline block entrance of PEG-*b*-PS diblock copolymer chains in crystalline structure in comparison to PEG-*b*-PMMA ones as well as making detectable height variances between different phase regions. Increasing the PS and PMMA blocks molecular weight, the dispersed domain sizes, due to enhancement of hindrance against presence of PEG-*b*-PMMA diblock copolymers in the single crystal structure, decreased. Due to lower osmotic pressure of PS tethered chains, the rising trend of thickness and tethering density via crystallization temperature was more significant in PS-covered regions in comparison with PMMA-covered ones. That is to say, raising the molecular weight, which belonged to one of amorphous blocks, the total and substrate thicknesses of the only related area underwent the variations. Additionally, in mixed-brush single crystals of PEG_{5000}-*b*-PS_{4600}/PEG_{5000}-*b*-$PMMA_{8700}$, the calculated thicknesses of PS phase regions and the PMMA disperses were equal to 7.7 and 4.0 nm respectively, and the corresponding achieved substrate thicknesses of epitaxial structure for PS and PMMA covered areas were somewhat the same.

Acknowledgments

The authors would like to extend our sincere gratitude to Prof. Ali Akbar Entezami and MarziehFathi who sympathetically helped us in synthesizing the materials. Our especial thanks also go to MortezaNasiri for his invaluable discussions on kinetic study.

Notes and references

1. Kind, H.; Yan, H.; Messer, B.; Law, M.; Yang, P. *Adv. Mater.* **2002**, *14*, 158.
2. Rosario, R.; Gust, D.; Hayes, M.; Jahnke, F.; Springer, J.; Garsia, A. A. *Langmuir* **2002**, *18*, 8062.
3. Lahann, J.; Mitragotri, S.; Tran, T. -N.; Kaido, H.; Sundaram, J.; Choi, I. S.;Hoffer, S.; Somorjal, G. A.; Langer, R. *Science* **2003**, *299*, 371.
4. Russel, T. P. *Science* **2002**, *297*, 964.
5. Yoshida, R.; Sakai, K.; Okano, T.; Sakurai, Y.; Bae, Y. H.; Kim, S. W. *J. Biomater. Sci. Polymer Edn.* **1991**, *3(2)*, 155.
6. Pan, V.; Wesley, R.; Lvginbuhl, R.; Denton, D.; Ratner, B. *Biomacromolecules***2001**, *2*, 32.
7. Nagasaki, Y.; Kataoka, K. *Trends Polym.Sci.* **1996**, *4*, 59.
8. deGennes, P. G. *Macromolecules* **1980**, *13*, 1069.
9. Sidorenko, A.; Minko, S.; Schenk-Meuser, K.; Duschner, H.; Stamm, M. *Langmuir* **1999**, *15*, 8349.
10. Usov, D.; Gruzdev, V.; Nitschke, M.; Stamm, M.; Hoy, O.; Luzinov, I.; Tokarev, I.; Minko, S. *Macromolecules* **2007**, *40*, 8774.
11. Zhou, F.; Huck, W. T. S. *Phys. Chem. Chem. Phys.* **2006**, *8*, 3815.
12. Advincula, R. C., Brittain, W. J., Caster, K. C., Rühe, J., Eds.; *Polymer Brushes;* Wiley-VCH: Weinheim**2004**.
13. Senaratne, W.; Andruzzi, L.; Ober, C. K. *Biomacromolecules* **2005**, *6*, 2427.
14. Jennings, G. K.; Brantley, E. L. *Adv. Mater.***2004**, *16*, 1983.
15. Tomlinson, M. R.; Genzer, J. *Chem. Commun.***2003**, 1350.
16. Dyer, D. J. *Adv. Funct.Mater.***2003**, *13*, 667.
17. Zhao, B.; Brittain, W. J. *Prog. Polym. Sci*. **2000**, *25*, 677.
18. Harris, B. P.; Kutty, J. K.; Fritz, E. W.; Webb, C. K.; Burg, K. J. L.; Metters, A. T. *Langmuir* **2006***, 22*, 4467.
19. Piehler, J.; Brecht, A.; Geckeler, K. E.; Gauglitz, G. *Biosensors and Bioelectronics* **1996***, 11*, 579.
20. Minko, S.; Patil, S.; Datsyuk, V.; Simon, F.; Eichhorn, K.-J.; Motornov, M.; Usov, D.; Tokarev, I.; Stamm, M. *Langmuir* **2002**, *18*, 289.
21. Idol, W. K.; Anderson, J. L. *J. Membr.Sci.* **1986**, *28*, 269.
22. Kim, J. U.; Matsen, M.W. *Eur. Phys. J. E.* **2007**, *23*,135.
23. Witten, T. A.; Pincus, P. A. *Macromolecules* **1986**, *19*, 2509.
24. Rouhi, A. M. *Chem. Eng. News* **1999**, *77*, 51.
25. Niklason, L. E.; Gao, J.; Abbott, W. M.; Hirschi, K. K.; Houser, S.; Marini, R.; Langer, R. *Science* **1999**, *284*, 489.
26. Kataoka, D. E.; Trolan, S. M. *Nature (London)* **1999**, *402*, 794.
27. Rouhi, A. M. *Chem. Eng. News* **1997**, *75*, 41.
28. Hesselink, F. T. *J. Colloid Interface Sci.* **1977**, *60*, 448.
29. Minko, S.; Usov, D.; Motornov, M.; Ionov, L.; Stamm, M. *Polym. Mater. Sci. Eng*. **2003**, 89, 156.
30. Zhao, B. *Polymer* **2003,** *44,* 4079.
31. Minko, S.; Usov, D.; Goreshnik, E.; Stamm, M. *Macromol. Rapid. Commun.* **2001**, *22*, 206.
32. Minko, S.; Müller, M.; Usov, D.; Scholl, A.; Froeck, C.; Stamm, M. *Phys. Rev. Lett.* **2002**, *88*, 035502.
33. Zhao, B.; Brittain, W. J. *Macromolecules* **2000**, *33*, 8813.
34. Minko, S.; Müller, M.; Motornov, M.; Nitschke, M.; Grundke, K.; Stamm, M. *J. Am. Chem. Soc.* **2003**, *125*, 3896.
35. Lemieux, M.; Minko, S.; Usov, D.; Stamm, M.; Tsukruk, V. V. *Langmuir* **2003**, *19*, 6126.
36. Wang, J.; Kara, S.; Long, T. E.; Ward, T. C. *J. Polym.Sci., Part A: Polym. Chem.* **2000**, *38*, 3742.
37. Chen, Y. Dissertation, University of Akron, **2005.**
38. Xiong, H.; Zheng, J. X.; Van Horn, R. M.; Jeong, K.-Un; Quirk, R. P.; Lotz, B.; Thomas, E. L.; Brittain, W. J.; Cheng, S. Z. D. *Polymer* **2007**, *48*, 3732.
39. Chen, W. Y.; Zheng, J. X.; Cheng, S. Z. D.; Li, C. Y.; Huang, P.; Zhu, L.; Xiong, H.; Ge, Q.; Guo, Y.; Quirk, R. P.; Lotz, B.; Deng, L.; Wu, C.; Thomas, E. L. *Phys. ReV. Lett.* **2004**, *93*, 028301.
40. Van Horn, R. M. Ph.D. Dissertation, University of Akron, **2009.**
41. Agbolaghi, S.; Abbasi, F.; Jalili, K. *Journal of Polym. Res.* **2014** (in press).
42. Chen, W. Y.; Li, C. Y.; Zheng, J. X.; Huang, P.; Zhu, L.; Ge, Q.; Quirk, R. P.; Lotz, B.; Deng, L.; Wu, C.; Thomas, E. L.; Cheng, S. Z. D. *Macromolecules* **2004**, *37*, 5292.

43. Zheng, J. X.; Xiong, H.; Chen, W.Y.; Lee K.; Van Horn, R. M.; Quirk, R. P.; Lotz, B.; Thomas, E.L.; Shi, A. -C.; Cheng, S. Z. D. *Macromolecules* **2006**, *39*, 641.
44. Brandup, J.; Immergut, E. H. Polymer Handbook; Wiley: New York, **1975.**
45. Wunderlich, B. *Macromolecular Physics* Vol. 1: Crystal Structure, Morphology, defects, Academic, New York, **1973**.
46. Weast, R. C. Handbook of Chemistry and Physics. New York: CRC Press; **1980**.
47. Walheim, S.; Boltau, M.; Mlynek, J.; Krausch, G.; Steiner, U. *Macromolecules* **1997**, *30*, 4995.
48. Jankova, K.; Chen, X. Y.; Kops, J.; Batsberg, W. *Macromolecules* **1998**, *31*, 538.
49. Xiao, Q.; Zhang, X.; Yi, J.; Wangand, X.; Zhang, H. *Iranian Polymer Journal* **2008**, *17*, 781.
50. Matyjaszewski, K.; Davis, T. P. Handbook of Radical Polymerization, Australia, By John Wiley and Sons, Inc., Hoboken, **2002**.
51. Reining, B.; Keul, H.; Hocker, H. *Polymer* **1999**, *40*, 3555.
52. Siegwart, D. J.; Wu, W.; Mandalaywala, M.; Tamir, M.; Sarbu, T.; Silverstein, M. S.; Kowalewski, T.; Hollinger, J. O.; Matyjaszewski, K. *Polymer* **2007**, *48*, 7279.
53. Jankova, K.; Chen, X. Y.; Kops, J.; Batsberg, W. *Polymer Bulletin* **1999**, *42*, 153.
54. Sun, X.; Zhang, H.; Huang, X.; Wang, X.; Zhou, Q. -F. *Polymer* **2005**, *46*, 5251.
55. Lotz, B.; Kovacs, A. J. *Kolloid Z. Z. Polym.***1966**, *209(2)*, 97.
56. Lotz, B.; Kovacs, A. J.; Bassett, G. A.; Keller, A. *Kolloid Z. Z. Polym.* **1966**, *209*, 115.
57. BaltáCalleja, F. J.; Hay, I. L.; Keller, A. *J. Polym.Sci.* **1964**, *A2*, 2171.
58. BaltáCalleja, F. J.; Hay, I. L.; Keller, A. *Colloid Z. Z. Polym. Sci.* **1966**, *209*, 128.
59. Chen, J.; Cheng, S. Z. D.; Wu, S. S.; Lotz, B.; Wittmann, J. -C. *J. Polym. Sci., Polym. Phys. Ed.* **1995**, *33*, 1851.
60. Hamie, H. Ph.D. Dissertation, University of Haute Alsace **2010**.
61. Richardson, P. H.; Richard, R. W.; Blundell, D. J.; MacDonald, W. A.; Mills, P. *Polymer***1995**, *36*, 3059
62. Taunton, H. J.; Toprakcioglu, C.; Fetters, L. J.; Klein, J. *Nature (London)* **1988**, *332*, 712.
63. Granick, S.; Herz, J. *Macromolecules* **1985**, *18*, 460.
64. Kent, M. S.; Lee, L. T.; Farnoux, B.; Rondelez, F. *Macromolecules* **1992**, *25*, 6240.
65. Bhushan, B.; Israelachvili, J. N.; Landman, U. *Nature (London)* **1995**, *374*, 607.
66. Milner, S. T. *Science* **1991**, *251*, 905.
67. Maul, J.; Frushour, B. G.; Kontoff, J. R.; Eichenauer, H.;Ott, K.-H.; Schade, C. Polystyrene and Styrene Copolymers; in Ullmann'sEncyclopedia of Industrial Chemistry, Wiley-VCH, Weinheim, **2007.**
68. Lauritzen, J. I.; Hoffman, J. D. *J. Res. Natl. Bur. Stand.***1960**, *64A*, 73.
69. Hoffman, J. D.; Lauritzen, J. I. *J. Res. Natl. Bur. Stand.***196**1, *65A*, 297.
70. Wunderlich, B. Macromolecular Physics; Academic Press: New York, **1980**.

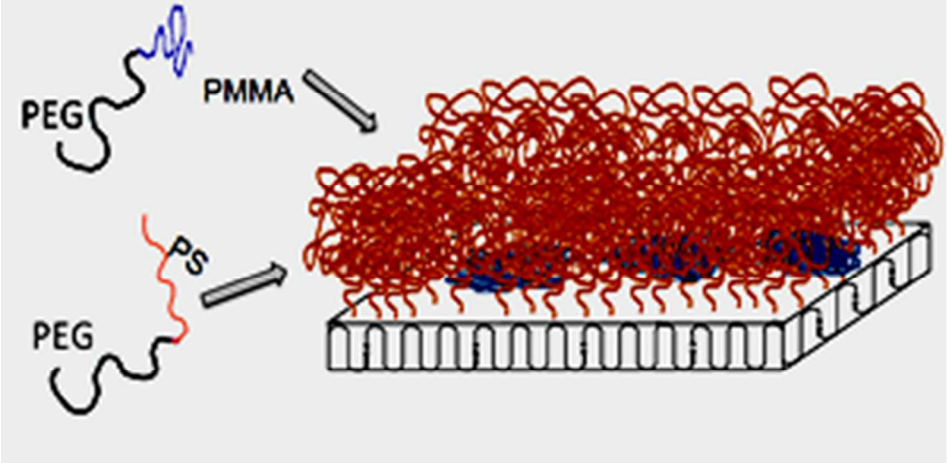

Single crystals having matrix-dispersed surface morphologies were prepared and characterized.
39x19mm (300 x 300 DPI)